Data Transfer in an Injection-Locked Oscillator Coupled to an External Resonator

Víctor Ardila, Franco Ramírez, Almudena Suárez

Departamento de Ingeniería de Comunicaciones, Universidad de Cantabria, Spain
ardilava@unican.es, ramirezf@unican.es, almudena.suarez@unican.es

***Abstract* — This work proposes the use of an injection-locked oscillator inductively coupled to an external resonator for power and data transfer. The injection locking prevents the variation of the oscillator carrier frequency with the coupling factor, while taking advantage of the oscillation to obtain high output power and efficiency under a low input amplitude. By using a rectifier, the inductively coupled oscillator can power a low-frequency source in the external resonator, which is used to modulate the oscillator signal. The high phase sensitivity of the locked regime enables a phase modulation through the variation of the external-resonator capacitance. This way data can be transmitted from the resonator to the oscillator, acting as a reader. A proof of concept has been implemented using a Class-E oscillator operating at 13.56 MHz, with good experimental results.**

***Keywords* — Injection locking, oscillator, inductive coupling.**

I. Introduction

Near-field wireless power transfer enables the short-distance recharge of implantable devices, sensor networks, and electrical car batteries, among other [1]-[3]. The transmitted power is generally obtained through a high-power amplifier driven by an input source. Alternatively, several works propose the use of a high-power oscillator [4]-[6], which reduces the number of components and the total energy consumption. However, the oscillation frequency depends [6] on the coupling factor between the oscillator inductor and the external-resonator inductor, as studied in detail in [7]. Thus, it will vary with the distance between the coils and their orientation, which may lead to operation outside the regulated frequency bands. To prevent this problem, the works [8]-[9] propose the injection locking of the oscillator by an external source. This avoids the variation of the oscillator carrier frequency, while taking advantage of this oscillation to obtain high output power and efficiency under a low input amplitude. In [8]-[9] a design procedure of the coupled injection-locked oscillator is presented, as well as an investigation of the effect of the external resonator elements on the locked solution curve(s) versus the coupling factor.

The previous works [8]-[9] consider the oscillator coupled to a simple RLC resonator. Here, for the first time, we will include a rectifier in the coupled resonator. With this rectifier, the injection-locked oscillator can power a low-frequency source, which will be used to modulate the oscillator signal. This way data can be transmitted from the resonator to the oscillator, acting as a reader. Because of the injection locking, phase modulations are possible; moreover, the phase noise will be much lower than that of the free-running oscillator [10]. Here the complete system will be analyzed through an extension of the method in [8], to obtain provide both the rectified voltage and the phase variation. The robustness of the data transmission under changes in the coupling factor will be analysed with envelope transient. Because the system is not optimized for data transfer, the aim is not to achieve a record performance, but to demonstrate the feasibility of the concept; this has been successfully applied to a Class–E oscillator at 13.56 MHz, which has been manufactured and measured.

II. Injection-Locked Oscillator

Under a small input amplitude, injection-locked oscillators inherently exhibit multiple steady state-solutions [11]. Default harmonic balance (HB) will converge to the lower-power solutions, in which the oscillation is not excited [11]. On the other hand, when continuously increasing the input amplitude, default HB will suffer from convergence problems or undergo discontinuous jumps due to the presence of turning points (points of infinite slope) in the solution curve. To cope with this problem, one can make use of a novel method, proposed in [8]. We will consider the Class-E oscillator at 13.56 MHz shown in Fig. 1(a), which is inductively coupled to an external resonator. The MOSFET drain DC voltage is 8 V, as recommended by the manufacturer. In the novel method, the input source is suppressed [Fig. 1(a)]. Instead, an auxiliary generator (AG) is introduced in the input network of the oscillator circuit. This generator, at the input frequency ω_g, can be of current or voltage type. A current (voltage) AG will have an ideal filter in parallel (series) to prevent the open (short) circuiting of the harmonic terms. The current (voltage) AG is used to extract a nonlinear impedance (admittance) that depends on the AG amplitude.

Together with the oscillator circuit excited by the AG, we simulate the linear input network comprised between the actual input source (E_g) and the AG [8]. The aim is to numerically obtain the Thevenin or Norton equivalent at the fundamental frequency. The two circuits are analysed simultaneously. In the case of the Class-E oscillator in Fig. 1(a), we have used a current AG, so the aim is to obtain the impedance function $Z_T(I_{AG}) = V_{AG}/I_{AG}$, where I_{AG} is the AG current amplitude and V_{AG} is the voltage drop across the AG. The second circuit is used to calculate a function able to provide the Thevenin voltage V_{Th} at the node where the current AG is connected. This is done by obtaining a frequency-dependent linear function F_{Th}, given by:

$$F_{Th} = V_{Th} / E_g \tag{1}$$

To calculate the above function, we excite the second (linear) network with a dummy source of value $E_g = 1$ V. Once we have

$Z_T(I_{AG})$ and F_{Th}, we can describe the system at the fundamental frequency through the following equation:

$$H(I_{AG}) = Z_T(I_{AG})I_{AG} / F_{Th} = E_g e^{j\phi} \qquad (2)$$

where the phase origin is taken at the branch current I_{AG}. Note that the oscillator circuit agrees with the original one at all the harmonic terms, due to the AG filter.

A. Power transfer curve

To obtain the power transfer curve of the injection-locked oscillator [8], we will perform a sweep in the current amplitude I_{AG} and calculate the input amplitude $|E_g|$ through:

$$\left|H(I_{AG})\right| = \left|Z_T(I_{AG})\right| I_{AG} / \left|F_{Th}\right| = \left|E_g\right| \qquad (3)$$

The above equation allows passing through all the possible turning points (infinite-slope points) obtained versus the input power. This is because we have performed a change in the analysis parameter: instead of $|E_g|$, we sweep the current I_{AG} (entering the device), with respect to which the system does not exhibit any singular points. In fact, the turning points will arise when representing I_{AG} versus $\left|H(I_{AG})\right| = \left|E_g\right|$, so the swept variable is in the vertical axis. The output power is obtained from the V_L value resulting from the sweep.

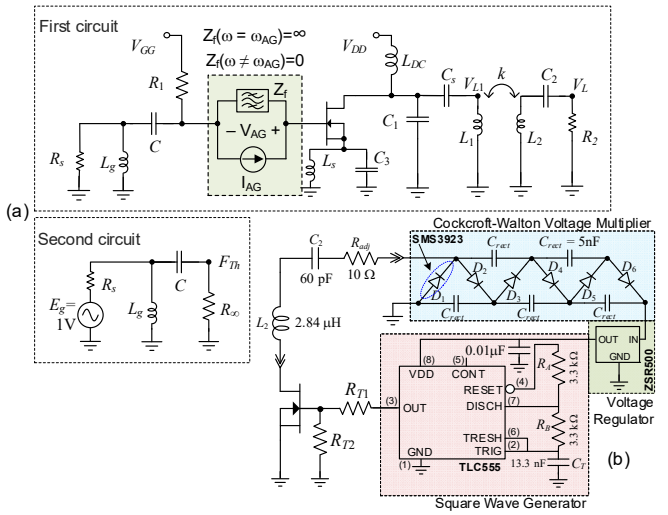

Fig. 1. Oscillator based on the MOSFET IRLML0040TRPbF coupled to an external resonator [8], with $C_2 = 55$ pF and $R_2 = 110$ Ω. (a) Simultaneous simulation of two circuits. The first circuit provides a numerical nonlinear impedance function Z_T at the AG location. The second circuit provides the linear function F_{Th} that enables the calculation of the Thevenin equivalent voltage V_{Th}. (b) External resonator including a three-stage voltage multiplier, a voltage regulator, and a square wave generator.

Fig. 2(a) compares the power transfer curves obtained under the coupling factor $k = 0.25$ in oscillatory and non-oscillatory conditions (without series feedback). When the circuit behaves as a free-running oscillator and the input frequency is 13.56 MHz, the circuit operates in a quasi-periodic regime until reaching the turning point T_1. This corresponds to a local-global bifurcation, at which injection locking takes place [12]. For input power $P_{in} > P_{in,T1}$, the circuit operates in the higher output-power section of the periodic solution curve, which is the only stable one. The results are compared with default HB simulations, unable to provide this higher power section in the presence of the coexisting lower power one (not shown due to the zoom). Default HB undergoes a discontinuous jump near the second turning point T_2. When the input frequency is closer to the free-running frequency (13.49 MHz), the oscillator gets locked at a much lower P_{in} (blue curve in Fig. 2(a), with a lower value of $P_{in,T1}$). For comparison, we also present the output power in non-oscillatory conditions, with the circuit behaving as a Class-E amplifier. Now, the lower power section of the curve is stable and when reaching the turning point T_2 there is a jump to the higher power section. When decreasing P_{in}, the jump takes place at T_1 in a hysteresis phenomenon. Again, default HB is unable to complete the solution curve. Fig. 2(b) presents the power transfer curves for different k values. The output power increases with k. There are also variations in $P_{in,T1}$, since the free-running oscillation frequency depends on k.

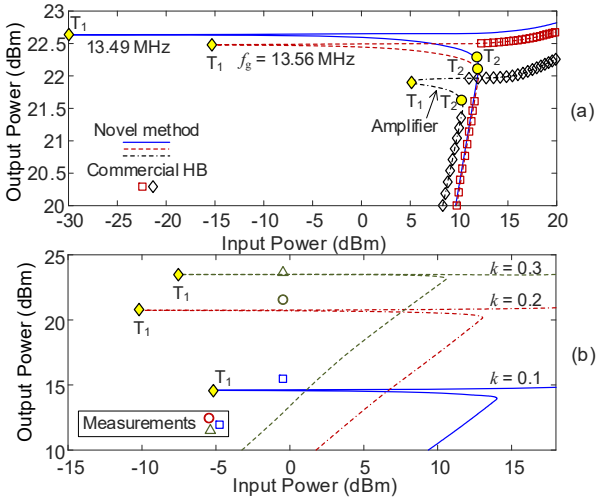

Fig. 2. Power-transfer curves. (a) $k = 0.25$, in oscillatory and non-oscillatory conditions. The results obtained with the novel method are compared with default HB. When the input frequency approaches the free running one, T_1 is obtained at a lower P_{in}. (b) $f_{in} = 13.56$ MHz and different k values.

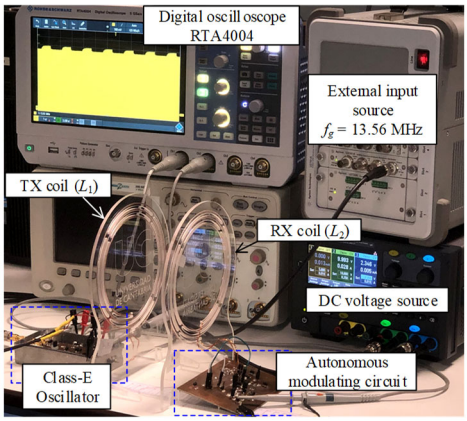

Fig. 3. Photograph of the measurement setup.

Fig. 3 shows the measurement setup, consisting of an input source, the Class-E oscillator, two coupled inductors (AWG-18 copper wire) on methacrylate and the external autonomous modulating circuit. The voltages at different nodes are measured with a R&S® RTA4K digital oscilloscope. Fig. 4(a)

and (b) present the measurement results in injection-locked mode and amplifier mode, in terms of output power and efficiency (compared with simulations). The measured efficiency in power transferred to R_2 is very high, due to the near-ideal MOSFET switching [in Fig. 3(c)]. In amplifier mode, no hysteresis is observed, which is attributed to modeling inaccuracies (there was agreement with default HB). As gathered from Fig. 2(a) and Fig. 4, the injection-locked oscillator provides high output power and efficiency from a much lower P_{in}. In Fig. 2(b), the measured output power for $P_{in} = -0.46$ dBm and different k values is superimposed.

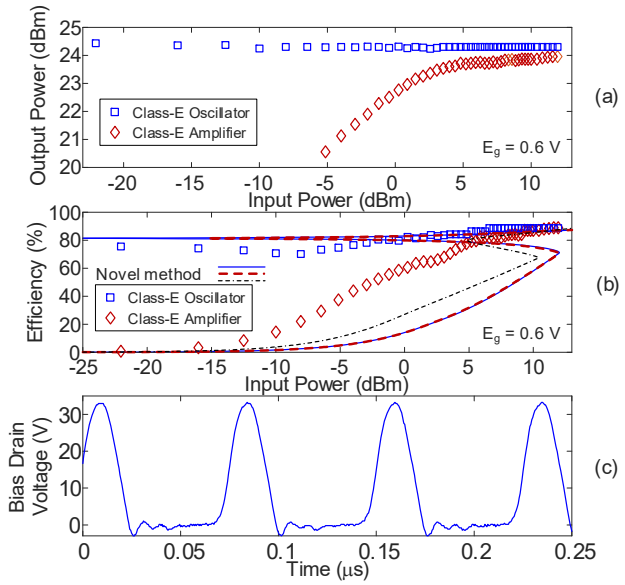

Fig. 4. Simulated and measured results at 13.56 MHz in injection-locked and amplifier modes. (a) Power. (b) Power-transfer efficiency. (c) Voltage waveform at the MOSFET drain node in uncoupled conditions.

B. Phase variation versus the capacitor C_2

For the data transfer, the aim is to modulate in phase the oscillator signal through the time variation of the external-resonator capacitance C_2. Before addressing the modulation, we will obtain the curve(s) that provide the oscillation phase versus C_2. This will be done for a particular input amplitude $|E_{go}|$, corresponding to $P_{in} = -0.46$ dBm. The analysis is carried out in two stages. First, we obtain solution curve(s) by performing a double sweep in C_2 and I_{AG} to calculate the function $H(C_2, I_{AG})$. Once H is available, the solution curve(s) is given by the constant-amplitude contour corresponding to $|E_{go}|$:

$$\left|H(C_2, I_{AG})\right| = \left|Z_T(C_2, I_{AG})\right| I_{AG} \,/\, \left|F_{Th}\right| = \left|E_{go}\right| \qquad (4)$$

Note that the above contour can be obtained directly in the output display of commercial HB. In a second step, we calculate the variation of the phase ϕ versus C_2 by interpolating the phase of H [see (2)] through the contour in (4), which is done in in-house software. The results obtained for $k = 0.25$ and $k = 0.35$ are shown in Fig. 5(a). One obtains two disconnected curves. The flat curve, which provides low output power [Fig. 5(b)], is unstable. The stable solutions correspond to the lower section of the higher output-power curve. The higher k (0.35) provides a larger phase excursion. As an intermediate step, we can trace in commercial HB a set of constant phase(H) contours in the same plane as (4) [Fig. 5(b)]. Note that the intersections of these contours with (4) provide the phase ϕ at valid solution points. This is because (due to the linearity of the input network) the device excitation is fully determined by the AG and the harmonic components see the original circuit.

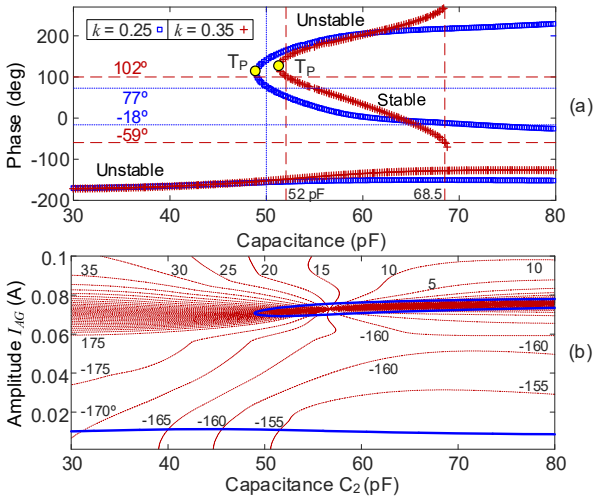

Fig. 5. Variation of the phase ϕ versus C_2. (a) Interpolation of phase(H) [in (2)] through the contour (4) obtained for $P_{in} = -0.46$ dBm. (b) Set of constant phase(H) contours traced in the same plane as (4) with commercial HB.

III. Analysis in the Presence of a Rectifier

In this work, we have analysed for the first time the injection-locked oscillator coupled to an external resonator including a rectifier. We have considered the three-stage voltage multiplier shown in Fig. 1(c). Because it is a proof of concept, no optimization of the complete external circuit has been carried out. To obtain the rectified voltage as a function of the coupling factor k, we have performed a double sweep in k and I_{AG} and calculated the contour:

$$\left|H(k, I_{AG})\right| = \left|Z_T(k, I_{AG})\right| I_{AG} \,/\, \left|F_{Th}\right| = \left|E_{go}\right| \qquad (5)$$

In addition, for each pair of values (k, I_{AG}) we have calculated the DC voltage V_{DC} in the output resistor of Fig. 1(b). In a manner similar to the phase analysis in Section II, using commercial HB we can trace contours of constant V_{DC} over the curve (5). In a second step, we have interpolated V_{DC} through the curve (5) using in-house software. This provides the rectified voltage and DC output power P_{DC} shown in Fig. 6. The upper section of the two curves (V_{DC} and P_{DC}) is stable except for a minor jump (between the two turning points) obtained at a relatively high k. The secondary circuit will now include three stages of the generator of Cockcroft–Walton connected in cascade (Greinacher multiplier), followed by a 5V regulation circuit. This energizes a 555 timer source in astable mode, configured to a duty cycle of 50% and an oscillation frequency of 14.5 kHz. The resulting square signal is shown in Fig. 7. For amplitude modulation, this signal feeds a switching transistor that disables or enables the receiving coil [Fig. 2(b)]. The resulting amplitude-modulated signal measured at the oscillator

(acting as a reader) is also shown in Fig. 7. For the phase modulation, the capacitor C_2 is replaced with a parallel arrangement of varactors (SMV1249) in antiseries connection. When introducing a rectangular signal between the diode terminals, one obtains the phase modulation presented in Fig. 5.

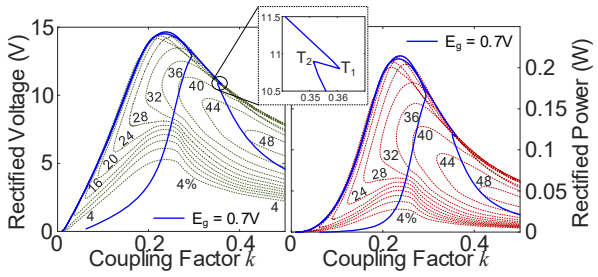

Fig. 6. Rectified voltage and DC output power P_{DC} versus k. The upper section of each curve is stable except for a minor jump (between the two turning points). The DC efficiency is overlapped (discontinuous line).

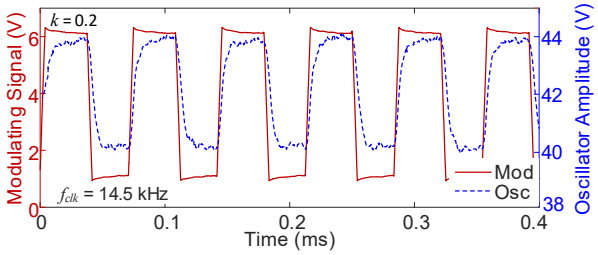

Fig. 7. Experimental signal obtained when connecting the rectifier output to a square-wave generator.

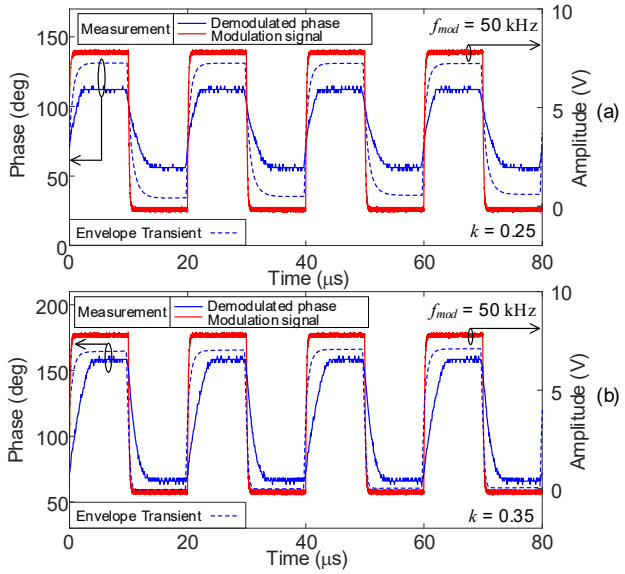

Fig. 8. Phase modulation for two different k values. The experimental phase waveform is compared with the one predicted by envelope transient and with the modulating rectangular signal. (a) k = 0.25 (3.5 cm). (b) k = 0.35 (2.5 cm).

In modulated conditions at a frequency of 50 kHz, the phase of the voltage V_{L1} in Fig. 1(a) is obtained through envelope transient. The phase variation for k = 0.25 (3.5 cm) is shown in Fig. 8(a). Note that the excursion (100º) approximately agrees with the one predicted in Fig. 5(a). The absolute values are different since Fig. 5(a) provides the opposite of the phase associated with I_{AG}, whereas Fig. 8(a) provides the phase of the voltage V_{L1}. The measured phase waveform is superimposed. Fig. 8(b) presents the simulated and experimental phase variations for k = 0.35 (2.5 cm). In this case the phase excursion is closer to 180º (164º) due to the smaller distance between the oscillator and the external resonator. Note that the maximum modulation frequency is limited by the time constants of the Class-E oscillator. A different oscillator design would enable higher modulation frequencies. The oscillator signal is demodulated by reading the voltage waveform at the coupled-inductor node, detecting th zero crossings with positive slope, and comparing them with the zero crossings of the locking signal. In comparison with the results of the amplitude-modulated free-running oscillator presented in [7] (based on the same design), the phase can be modulated at a higher frequency. Variations up to 100 kHz were detectable.

IV. Conclusion

A first conceptual demonstration of an injection-locked oscillator coupled to an external resonator for data transfer has been presented. It has been analyzed through a HB method based on the calculation of a nonlinear impedance function, plus the Thevenin equivalent of the input network. This enables the analysis of the phase sensitivity to the resonator capacitor and the prediction of the rectified voltage. The oscillator phase is modulated through the time variation of the external resonator capacitance, implemented through varactor diodes.

References

[1] J. Garnica, R. A. Chinga, and J. Lin, "Wireless power transmission: From far field to near field," *Proc. IEEE*, vol. 101, no. 6, pp. 1321–1331, 2013.

[2] S. R. Khan, S. K. Pavuluri, M. P. Y. Desmulliez, "Accurate Modeling of Coil Inductance for Near-Field Wireless Power Transfer," *IEEE Trans. Microw. Theory Tech.*, vol. 66, no. 9, pp. 4158–4169, Sep. 2018.

[3] O. Abdelatty, X. Wang, and A. Mortazawi, "Position-Insensitive Wireless Power Transfer Based on Nonlinear Resonant Circuits," *IEEE Trans. Microw. Theory Tech.*, vol. 67, no. 9, pp. 3844–3855, Sep. 2019.

[4] A. Jarndal and T. Petrovic, "GaN-Based Oscillators for Wireless Power Transfer Applications," *2018 Int. Conf. Adv. Comp. Telecom.*, Dec. 2018.

[5] A. Costanzo, M. Dionigi, F. Mastri, and M. Mongiardo, "Rigorous modeling of mid-range wireless power transfer systems based on royer oscillators," *2013 IEEE Wirel. Power Transf. WPT*, pp. 69–72, 2013.

[6] F. Mastri, A. Costanzo, M. Dionigi, M. Mongiardo, "Harmonic balance design of wireless resonant-type power transfer links," *2012 IEEE MTT-S Int. Microw. Workshop Series on Innovative Wireless Power Trans.: Techn., Systems, and App.*, Kyoto, Japan, 2012, pp. 245-248

[7] V. Ardila, F. Ramirez, and A. Suarez, "Nonlinear Dynamics of an Oscillator Inductively Coupled to an External Resonator for Power Transfer and Data Transmission," *IEEE Trans. Microw. Theory Tech.*, vol. 70, no. 4, pp. 2418–2431, Apr. 2022.

[8] V. Ardila, F. Ramirez, and A. Suarez, "Nonlinear Analysis of an Injection-Locked Oscillator Coupled to an External Resonator," *IEEE Microw. Wirel. Components Lett.*, vol. 36, no. 6, pp. 740-743, Jun., 2022.

[9] V. Ardila, F. Ramírez, A. Suárez, "Analysis and Design of Injection-Locked Oscillators Coupled to an External Resonator," *IEEE Trans. Microw. Theory Techn.*, vol. 71, 2023.

[10] S. Kalia, M. Elbadry, B. Sadhu, S. Patnaik, J. Qiu and R. Harjani, "A simple, unified phase noise model for injection-locked oscillators," *2011 IEEE RFIC Symposium*, 2011.

[11] A. Suárez, *Analysis and design of autonomous microwave circuits*, IEEE-Wiley, New Jersey, 2009.

[12] J. Guckenheimer and P. J. Holmes, *Nonlinear Oscillations, Dynamical Systems, and Bifurcations of Vector Fields*, vol. 42. 1983.